0254-6124/2026/46(5)-0001-16 *Chin. J. Space Sci.* 空间科学学报

HUANG Cong, LV Jingtian, LI Jiawei, SHEN Guohong, WANG Chunqin, ZHANG Shenyi, WANG Jingdong, KONG Linggao, LIU Chao, ZHANG Binquan, ZOU Hong, YU Xiangqian, WANG Xinyue, LIU Bin, WANG Yongfu, LIU Ying, YE Shanzhi, ZHANG Yiteng, XIAO Chijie, ZHANG Xianguo, ZONG Weiguo. In-orbit Validation of SEM-II onboard FengYun-3E. *Chinese Journal of Space Science*, 2026, **46**(5): 1–16. CSTR:32142.14.cjss.2025–0226. DOI:10.11728/cjss2026.05.2025–0226

In-orbit Validation of SEM-II onboard FengYun-3E*

HUANG Cong[1,2] LV Jingtian[1,2] LI Jiawei[1,2] SHEN Guohong[3,4]
WANG Chunqin[3,4] ZHANG Shenyi[3,4] WANG Jingdong[3,4] KONG Linggao[3,4]
LIU Chao[3,4] ZHANG Binquan[3,4] ZOU Hong[5] YU Xiangqian[5] WANG Xinyue[3,4]
LIU Bin[3,4] WANG Yongfu[5] LIU Ying[5] YE Shanzhi[3,4] ZHANG Yiteng[3,4]
XIAO Chijie[5] ZHANG Xianguo[3,4] ZONG Weiguo[1,2]

1(*Key Laboratory of Space Weather*, *National Satellite Meteorological Center* (*National Center for Space Weather*), *China Meteorological Administration*, *Beijing* 100081)

2(*Innovation Center for FengYun Meteorological Satellite* (*FYSIC*), *Beijing* 100081)

3(*National Space Science Center*, *Chinese Academy of Sciences*, *Beijing* 100190)

4(*Beijing Key Laboratory of Space Environment Exploration*, *Beijing* 100190)

5(*School of Earth and Space Sciences*, *Peking University*, *Beijing* 100871)

Abstract The new generation of Space Environment Monitor (SEM), SEM-II, onboard the Chinese meteorological satellite, FengYun-3E, has the ability to measure the charged particle flux with particle energy from 30 eV to 300 MeV in multi-directions, the satellite surface potential, the radiation dose in sensors, and the geomagnetic field variations. The space environment detections derived from SEM-II can be utilized for satellite security designs, scientific studies, development of radiation belt models, and space weather event monitoring or disaster warning. In this paper, we introduce the SEM-II's instrument characteristics, interpret the in-orbit calibration algorithm, perform the quantitative test to check the particle and the magnetic field detections' biases by the cross-calibration methods, and do the qualitative tests to check whether the radiation dose and the surface potential detections follow the nature law of space environment by comparing with the historical records. The results show that the uncertainties of the particle detections are less than 20%, the uncertainties of the magnetic field detections are about 1%, the radiation dose and the surface potential detections coincide with the historical records and the space environment knowledge. The instruments' responses to the space weather events are also presented.

Key words FengYun-3E, Space environment, Radiation effects, Energetic particles, Space technology

Classified index V524.3

0 Introduction

The Space Environment Monitor-II (SEM-II) onboard FengYun-3E (FY-3E) meteorological satellite is an updated version of the SEM-I onboard the previous FY-3 series satellites[1–3]. FY-3E was successfully launched

* Supported by the National Key Research and Development Program of China (2022YFB3901802) and the National Natural Science Foundation of China (No. 42074223)

Received December 23, 2025. Revised May 27, 2026

©The Author(s) 2026. This is an open access article under the CC-BY 4.0 License (https://creativecommons.org/licenses/by/4.0/)

Table 1 Instruments specifications of FY-3E/SEM-II

Instrument name	Observation object	Installation geometry	Sampling rate	Sensitivity	Channels
High energy particles detector	Integrated particle flux	3 directions in *–X/Y/-Z* with each direction's view field ~ 40°	0.5 Hz	5% ($\Delta N/N$)	6 energy bands for proton in 3-300 MeV; 5 energy bands for electron in 0.15-5.7 MeV
Medium energy proton detector	Integrated proton flux	18 directions with each direction's view field ~ 20°	0.5 Hz	5% ($\Delta N/N$)	12 energy bands for proton in 30 -5000 keV
Medium energy electron detector	Integrated electron flux	18 directions with each direction's view field ~ 20°	0.5 Hz	5% ($\Delta N/N$)	8 energy bands for electron in 30-600 keV
Radiation dose detector	Total radiation dose	3 probes installed on the interior surface of the outer wall of the satellite in *X/Y/-Z*	1/60 Hz	2 rad (Si)	Each probe has 2 channels: one's range is for 3×10^4 rad (Si), the other's range is for 5×10^3 rad (Si)
Surface potential detector	Surface potential	Relative Surface Potential Detector (RSPD) has 2 detectors: one faces to the night side, the other faces to the day side; Absolute Surface Potential Detector (ASPD)'s detail can be found in section 1.1.5	0.5 Hz	<15 V	RSPD has 2 channels; ASPD's channels are illustrated in Figure 3
Magnetic field detector	Magnetic field	6 sensors deployed on the satellite's truss	50 Hz	0.1 nT	Each sensor has three orthogonal channels to detect the magnetic field vectors

into orbit on 5 July 2021, which is the new Chinese operational meteorological satellite in Sun-synchronous polar circle Low-Earth-Orbit (LEO, about 830 km) with a 98° inclination, covering the dawn-dusk orbit. SEM-II booted up on 10 July 2021 and keeps in normal operation so far. This new generation of SEM, SEM-II, has new abilities to measure the charged particle flux with particle energies from 30 eV to 300 MeV in multi-directions, the satellite surface potential, the radiation dose in sensors, and the geomagnetic field variations. The measurements of the space radiation environment can be used in the area of satellite security designs, scientific studies, development of radiation belt models, space weather event monitoring or disaster warning, and supporting the Chinese manned spaceflight missions[1].

In the period from July to December 2021, we performed the in-orbit test of SEM-II to check the particle and magnetic field detections biases by cross-calibration methods and whether the radiation dose and surface potential detections follow the nature law of the space environment by comparing with the historical records.

1 Instruments Description

FY-3E is observing the Earth from the Sun-synchronous orbit and passing the ascending node at 17:40 LT and the descending node at 05:40 LT. The orbital period is about 102 minutes with the approximate altitude at 830 km. The SEM-II onboard FY-3E has the capacity to measure the flux of charged particles (protons and electrons) into the upper atmosphere, detect the geomagnetic field, and monitor the satellite surface potential and radiation dose in sensors.

It should be noted that, in FY-3E's satellite coordinate system, *X* is in the direction of the satellite velocity, *Z* is the direction to the Earth center, *Y* is perpendicular to the *XZ* plane and points to the night side.

1.1 Particle Detectors

The particle detectors have passed the ground tests using an accelerator and radiation source, and meet the calibration requirements from the simulation signals during the prelaunch period[4].

1.1.1 High Energy Particles Detector (HEPD)

SEM-II HEPD has two groups of detectors for detecting protons and electrons, respectively. Each group contains three directional detectors which are pointing to *-X/Y/-Z* directions in the satellite coordinate. The proton detectors can measure the proton flux in 6 energy bands: 3-5 (P1), 5-10 (P2), 10-26 (P3), 26-40 (P4), 40-100 (P5),

and 100-300 (P6) MeV. The electron detectors can measure the electron flux in 5 energy bands: 0.15-0.35 (E1), 0.35-0.65 (E2), 0.65-1.20 (E3), 1.20-2.00 (E4), and 2.00-5.70 (E5) MeV.

1.1.2 Medium Energy Proton Detector (MEPD)

SEM-II MEPD has the abilities to detect the medium energy proton flux *in situ* in 18 directions in the satellite coordinate (see the details in Figure 1). The proton energy is from 30 keV-5 MeV in 12 energy bands: 30-48 (P1), 48-80 (P2), 80-120 (P3), 120-170 (P4), 170-240 (P5), 240-350 (P6), 240-350 (P7), 350-500 (P8), 500-800 (P9), 800-1500 (P10), 1500-3000 (P11), 3000-5000 (P12) keV. There are two parts in the MEPD design: a low-energy part and a high-energy part. The energy bands from P1 to P6 belong to the low-energy part, while the other energy bands belong to the high-energy part. The designers set P6 and P7 as the overlap channels (240-350 keV) to check the consistency of detection.

1.1.3 Medium Energy Electron Detector (MEED)

SEM-II MEED has the abilities to detect the medium energy electron flux *in situ* in 18 directions in the satellite coordinate (see the details in Figure 2). The electron energy is from 30 to 400 keV in 8 energy bands: 30-40 (E1), 40-60 (E2), 60-90 (E3), 90-130 (E4), 130-190 (E5), 190-280 (E6), 280-410 (E7), 410-600 (E8) keV.

1.1.4 Radiation Dose Detector (RDD)

SEM-II RDD has the abilities to detect the radiation dose *in situ* in *X/Y/-Z* directions in the satellite coordinate with two channels in each direction. The detection sensitivity is better than 2 rad (Si) and the measurement uncertainty is within 10% based on the prelaunch calibration test.

1.1.5 Surface Potential Detector (SPD)

SEM-II SPD contains two parts: Relative Surface Potential Detector (RSPD) and Absolute Surface Potential Detector (ASPD). These detectors have the abilities to detect the surface potentials of the satellite on both dayside and nightside (see Figure 3). The relative surface potentials are retrieved from the volt changes in the detectors and the absolute surface potentials are derived

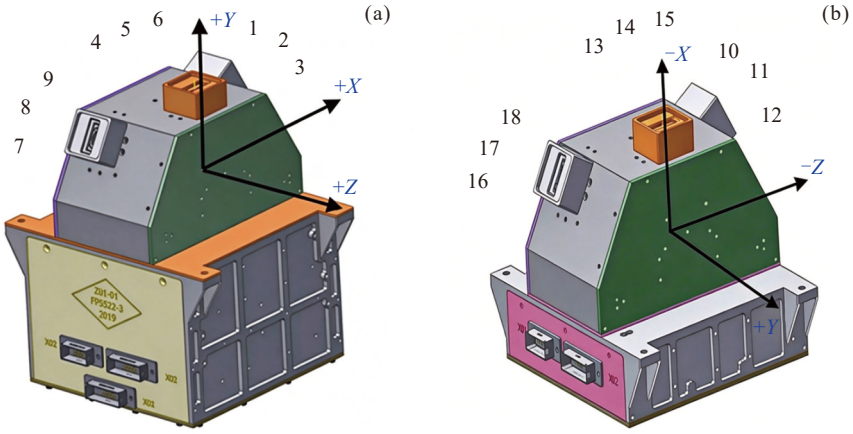


Fig. 1 SEM-II MEPD directions map

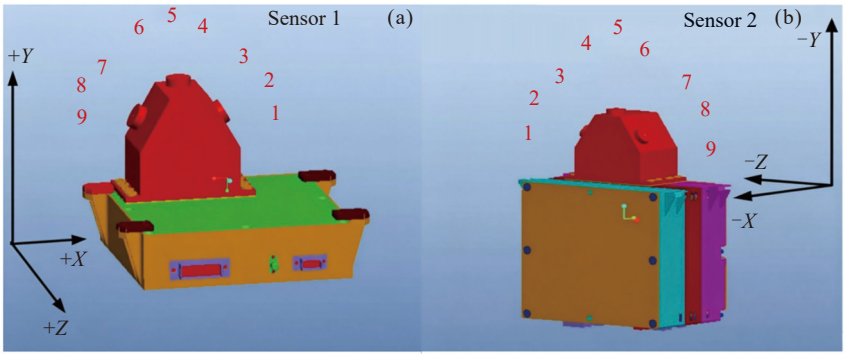


Fig. 2 SEM-II MEED directions map (Left is Sensor 1, Right is Sensor 2)

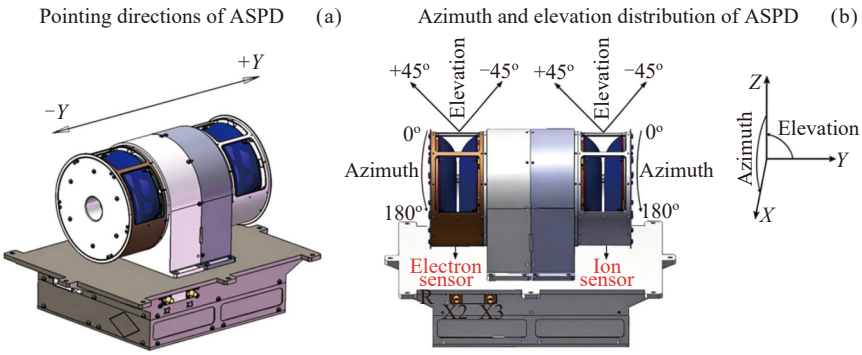


Fig. 3 SEM-II ASPD directions map

from the energy spectrums (30 eV-30 keV) of the plasma surrounding the satellite. The potential detections uncertainty is within 20% based on the prelaunch calibration test.

1.1.6 Magnetic Field Detector (MFD)

SEM-II MFD has the abilities to detect the magnetic field vectors *in situ* in the satellite orbit without rods (see Figure 4). After excluding the satellite remanence, we can retrieve the geomagnetic field changes from the detections. The time resolution of the detections is 1 s and the detections uncertainty is 1 nT based on the prelaunch calibration test.

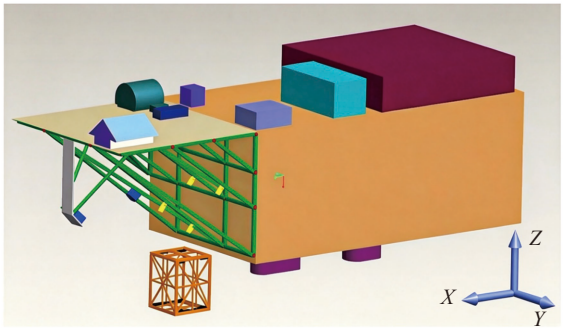


Fig. 4 SEM-II MFD assembly map, the yellow (GMR, Giant Magneto Resistive) and blue blocks (FGM, Flux Gate Magnetometer) on the satellite truss (green) indicate where the six sensors are deployed

2 In-orbit Testing Approach

We apply the qualitative test and the quantitative test to identify the validity of SEM-II detections. For the qualitative test, we check if the SEM-II detections follow the space environment rules. To the quantitative test, we do the inter-comparisons with other satellite detections or model results to check the validity of SEM-II detections.

3 In-orbit Testing Results

3.1 Energetic Particle Detections

Energetic particle detections include the detections from HEPD, MEPD and MEED.

3.1.1 Qualitative Test

In Figure 5, (a) is for the proton energy of 26-40 MeV in -*X* direction; (b) is for the electron energy of 0.65-1.20 MeV in -*X* direction; (c) is for the proton energy of 120-170 keV in the 4 th direction of Figure 1; (d) is for the electron energy of 90-130 keV in the 4 th direction of the sensor 1 in Figure 2. The approach for the maps generation: we generate a 360°(longitude)×180°(latitude) matrix, the data from the detection points located within a 0.5°range (*i.e.*, 1°grid) around each latitude and longitude point is averaged as the detection result for that latitude and longitude point . From Figure 5, we can find that the particle detections from SEM-II show the South Atlantic Anomaly (SAA) region at low latitudes and the outer radiation belt at high latitudes clearly. These radiation belt patterns and the particle directional flux distributions agree well with our space environment knowledge.

3.1.2 Quantitative Test

To the quantitative test of particle detections, we perform the inter-comparisons with the POES (Polar Orbiting Environmental Satellite) satellite particle detections from MEPED (Medium Energy Proton and Electron Detector) onboard POES N-19. We chose the same period (about a month) of detections and, for each satellite, the data from the detection points located within a 0.5 °

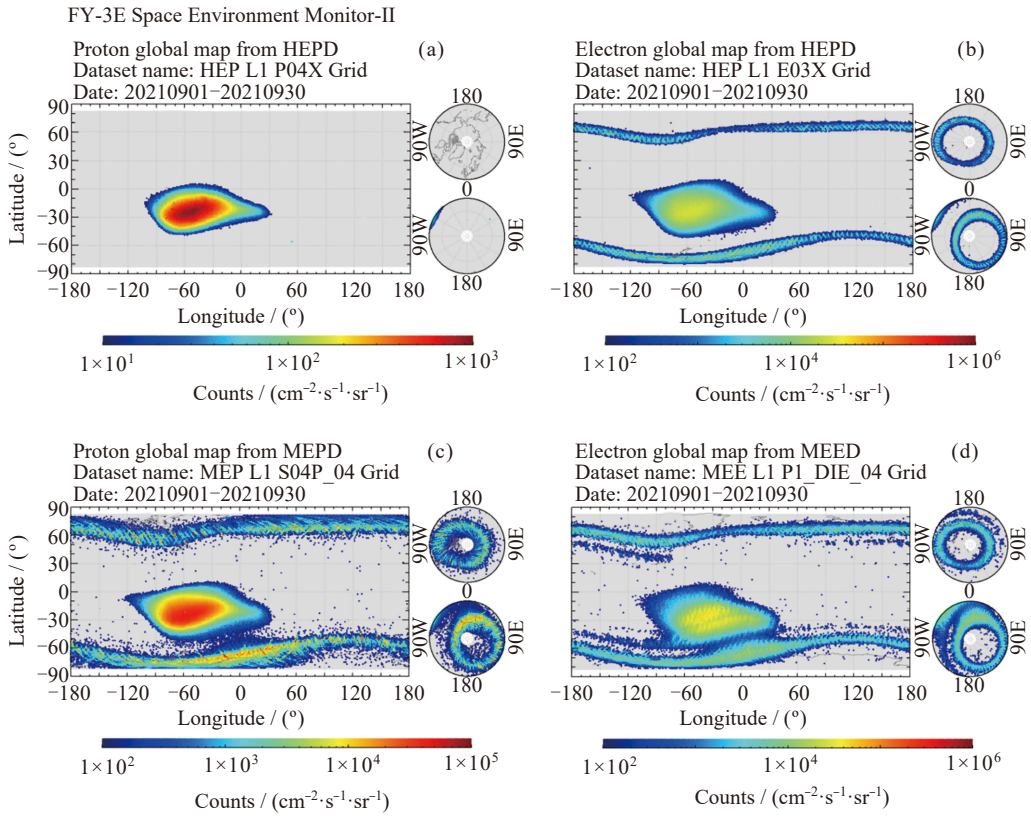


Fig. 5 Radiation belt detections from SEM-II

range (*i.e.,* 1°grid) around each latitude and longitude point is averaged as the detection result for that latitude and longitude point. We compared two satellite detections at the same latitude and longitude position. Due to that the energy bands of MEPED are different from SEM-II, we do the power-law fitting[5] to derive the particle spectrum or combine the two datasets to the same energy bands. Considering the particle anisotropy and the differences in pitch angle between two datasets, we select the particles with close pitch angles (absolute value of the pitch angle difference is less than 10°) in the inter-comparison works. More details can be found in Huang *et al*[1]. We set F as the particle flux (it is the linear flux, not the logarithmic flux in the calculation) in a certain energy band and mean(•) is the average operation on the dataset, set the Standard Deviation (STD, δ_{STD}) is $\delta_{\mathrm{STD}} = \{\mathrm{mean}\left[(F_{\mathrm{FY\text{-}3\,E}} - F_{\mathrm{N\text{-}19}})^2\right]\}^{0.5}$, the average relative deviation (ASTD, σ_{STD}) is $\sigma_{\mathrm{STD}} = \delta_{\mathrm{STD}}/\mathrm{mean}(F_{\mathrm{N\text{-}19}})$. The comparison results are shown in Figure 6. In Figure 6, (a)-(c) are for the results of HEPD and MEPD where the different colors denote the different periods; (d) is for the results of MEED in September, 2021. From Figure 6, it can be calculated that the total relative biases of the particle detections between SEM-II and MEPED are less than 25%. Table 2 illustrates the specific statistical information of the test results in Figure 6.

3.2 Magnetic Field Measurements

Magnetic field measurements are derived from MFD.

3.2.1 Qualitative Test

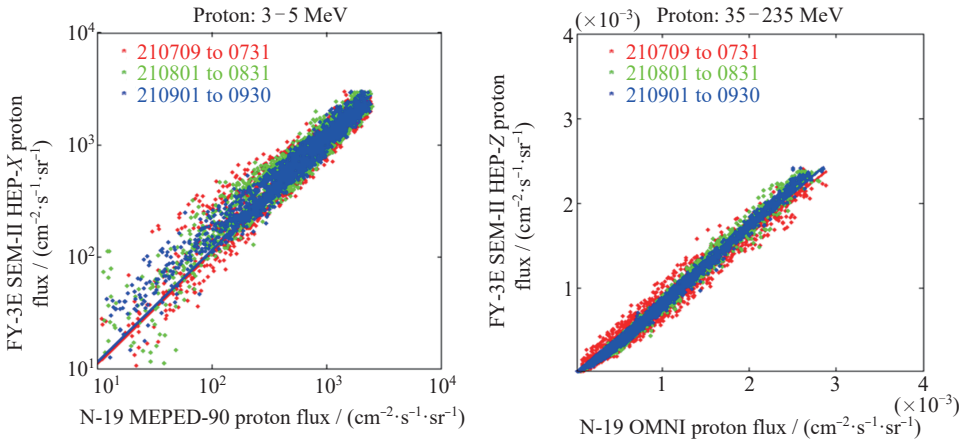
Figure 7 shows the magnetic field intensities at the FY-3E orbit and the magnetic field distribution coincides with our geomagnetic knowledge. The negative magnetic field region in SAA and the high value regions at high latitudes are clearly described in Figure 7(a). Figure 7(b) shows the geomagnetic field distributions from SEM-II compared with IGRF13.

3.2.2 Quantitative Test

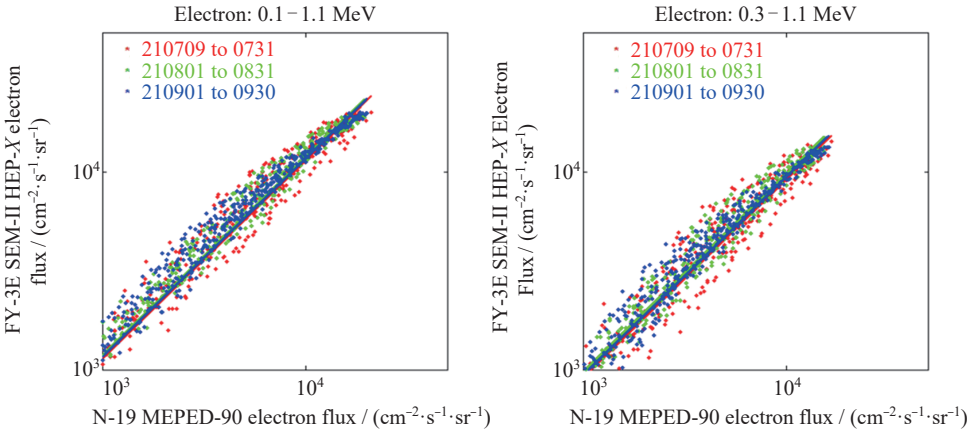
For the quantitative test of magnetic field measurements, we compare the measurements from SEM-II with IGRF13 (International Geomagnetic Reference Field 13 th) model. We use IGRF13 as a reference and output the model calculation values of IRGF13 at each detection point (spatial position) for comparison with the

magnetic field detection data of FY-3E. We use the total field data, B_T, and set the Bias=($B_{T,\ Sensor}$–$B_{T,\ IGRF}$)/B_T to calculate the bias between FY-3E/SEM-II and IGRF13. The dataset period is in August, 2021 and the sample size is about 2.2×10^6 (exact 1 Hz samples from the 50 Hz detections). In Figure 8, IGRF (IGRF13) is used as the reference and the bias is calculated by ($B_{T,\ Sensor}$–$B_{T,\ IGRF}$)/$B_{T,\ IGRF}$, 3% in (a) is the deviation_check line, Sensors include WG1-4 and FGM1-2, FGM*x* denotes the sensors based on flux-gate magnetometer technology and WG*x* denotes the sensors based on GMR (Giant Magneto Resistive) technology. The results are shown in Figure 8 and it is found that the total biases between SEM-II and IGRF13 are approximately 1%.

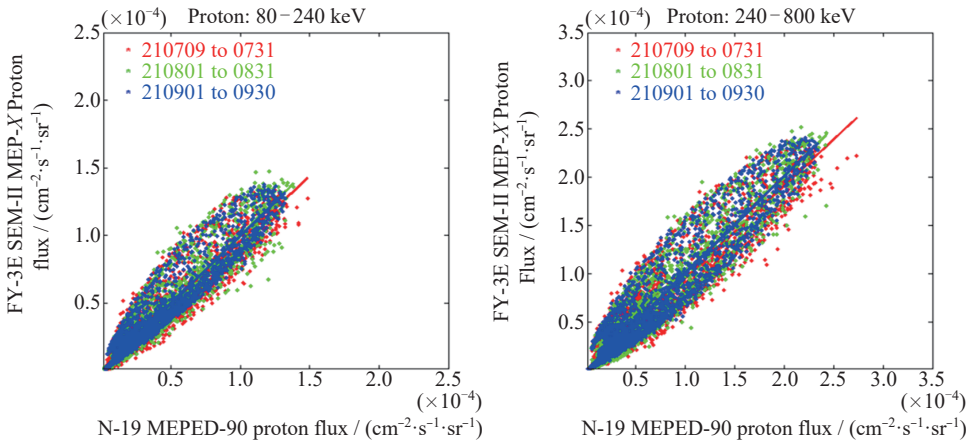
(a) Proton inter-comparisons of FY-3E_SEM-II_HEPD *vs*. N-19_SEM_MEPED



(b) Electron inter-comparisons of FY-3E_SEM-II_HEPD *vs*. N-19_SEM_MEPED



(c) Proton inter-comparisons of FY-3E_SEM-II_MEPD *vs*. N-19_SEM_MEPED



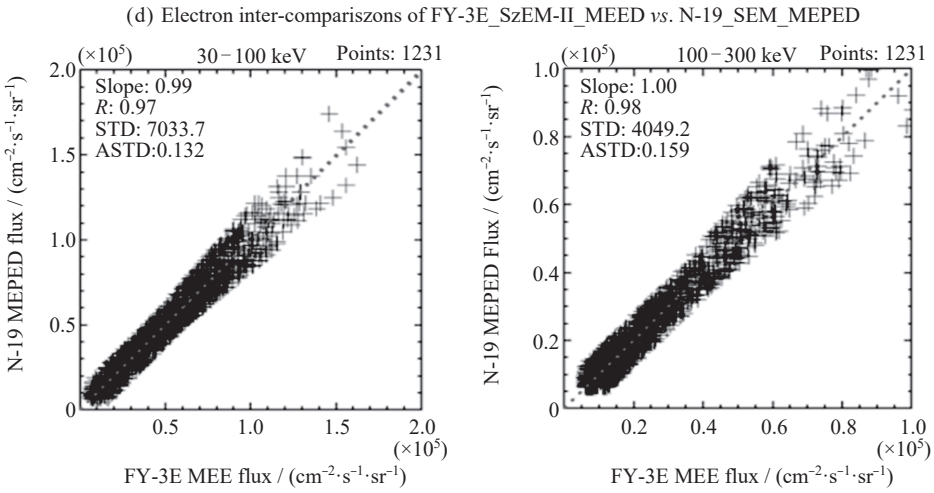


Fig. 6 Particle inter-comparisons of FY-3E *vs.* N-19

Table 2 Statistics for the particle inter-comparisons (FY-3E *vs.* N-19) in Fig. 6

Time	Correlation coefficient	Slope	Average Relative Deviation (ASTD)	Spots number
FY-3E HEP –*X vs.* N-19 MEPED90: 3-5 MeV				
Jul. 2021	0.94	1.10	20.22%	1971
Aug. 2021	0.95	1.15	23.35%	1957
Sept. 2021	0.96	1.15	20.39%	1953
FY-3E HEP –*Z vs.* N-19 OMNI: 35 - 275 MeV				
Jul. 2021	0.99	0.93	19.92%	2065
Aug. 2021	0.99	0.86	17.03%	2077
Sept. 2021	0.99	0.85	17.74%	2077
FY-3E HEP –*X vs.* N-19 MEPED90: 0.1 - 1.1 MeV				
Jul. 2021	0.96	1.14	23.46%	325
Aug. 2021	0.98	1.19	24.60%	326
Sept. 2021	0.99	1.17	24.41%	442
FY-3E HEP –*X vs.* N-19 MEPED90: 0.3 - 1.1 MeV				
Jul. 2021	0.96	0.92	17.75%	325
Aug. 2021	0.97	0.98	13.13%	326
Sept. 2021	0.99	0.94	10.88%	442
FY-3E MEP –*X vs.* N-19 MEPED90: 80 - 240 keV				
Jul. 2021	0.92	0.86	24.69%	1600
Aug. 2021	0.93	0.91	23.85%	1714
Sept. 2021	0.94	0.93	21.38%	1837
FY-3E MEP –*X vs.* N-19 MEPED90: 240-800 keV				
Jul. 2021	0.95	0.99	20.87%	2089
Aug. 2021	0.96	1.05	20.04%	2040
Sept. 2021	0.96	1.05	19.29%	2101

续表 2

Time	Correlation coefficient	Slope	Average Relative Deviation (ASTD)	Spots number
FY-3E MEE *vs.* N-19 MEPED00: 30-100 keV				
Sept. 2021	0.97	0.99	13.2%	1231
FY-3E MEE *vs.* N-19 MEPED90: 100-300 keV				
Sept. 2021	0.98	1.00	15.9%	1231

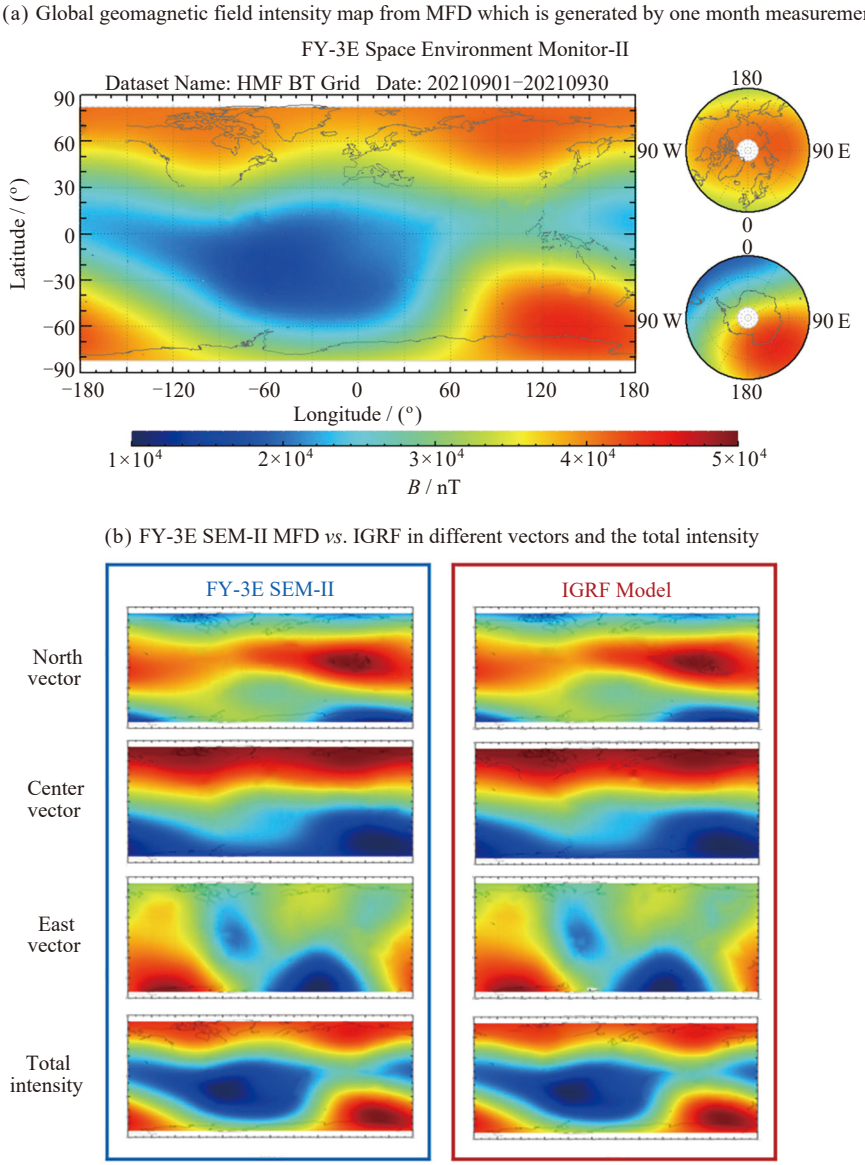


Fig. 7 Geomagnetic field map from FY-3E_SEM-II_MFD compared with IGRF13. The way for these maps' generation is like that in Fig. 5

3.3 Radiation Effect Observations

Radiation effect observations include the detections from RDD and SPD.

3.3.1 Qualitative Test

Figure 9 shows the radiation dose increasing. It is found that the radiation dose increasing rates are different in different directions. The increasing rate in Y direction is fastest. This situation coincides with the space radiation theory due to that the particle intensity is higher in Y direction when the pitch angle is close to 90°. The radiation dose

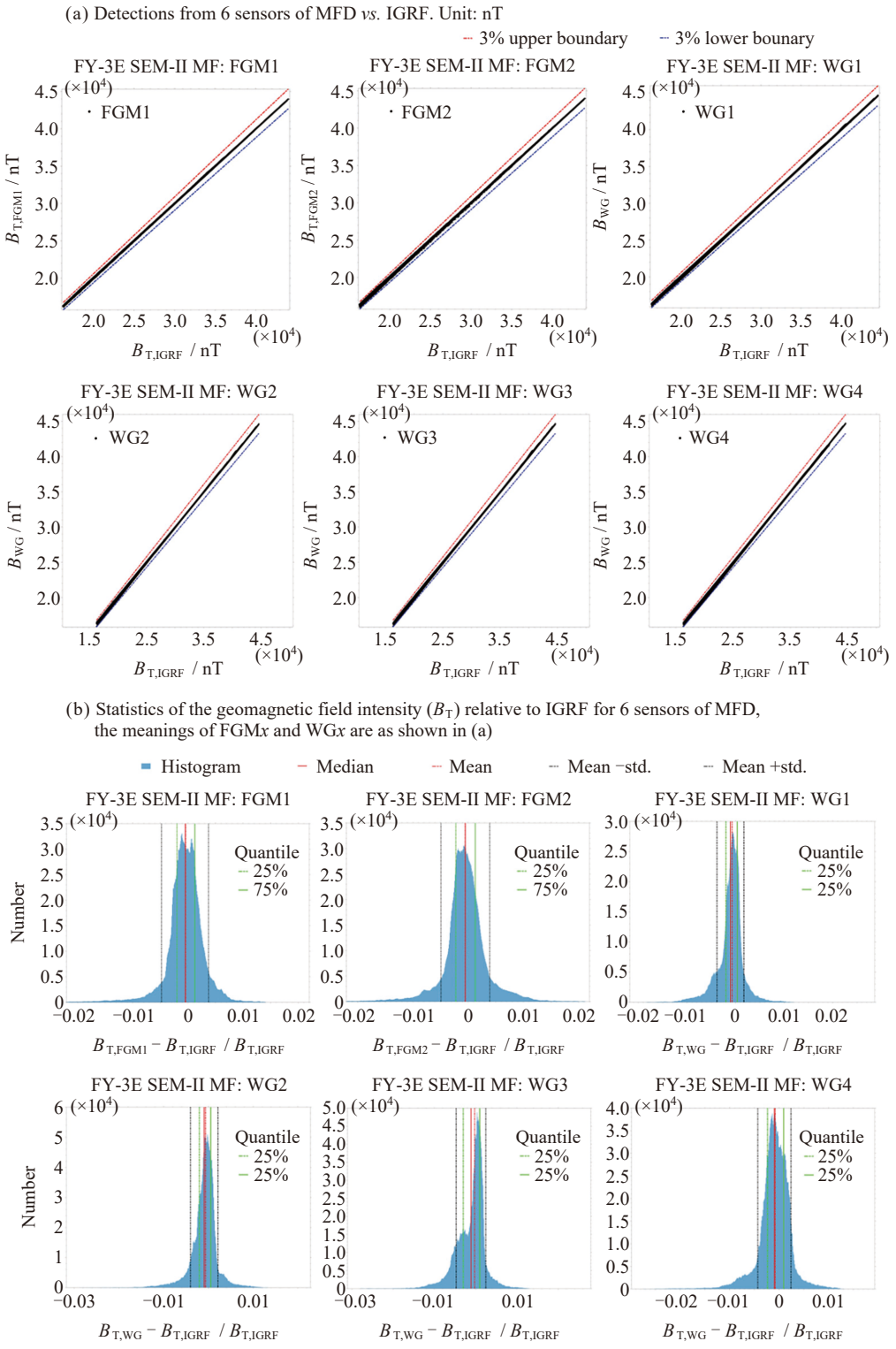


Fig. 8 Quantitative comparisons of the total intensity between FY-3E_SEM-II_MFD and IGRF in August 2021

increasing rate shows good responses to several geomagnetic storms that occurred at the end of August 2021, the end of October 2021, and the middle of January 2022.

Figure 10(a)(b) show the time series and the global distribution of the observations from RSPD. During the in-orbit testing period, the surface charging volt reaches –80 V and the charging events concentrate in the outer radiation belt at high southern latitudes. These features

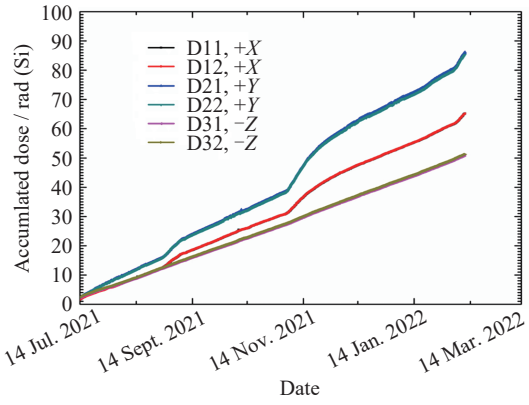


Fig. 9 Radiation dose detected by FY-3E_SEM-II_RDD, the different colors denote the accumulated radiation dose from the different sensors in *X*/*Y*/-*Z* directions

of RSPD onboard FY-3E agree well with the previous detections from FY-3D (Figure10 c). Figure 11 shows the plasma particle detections from ASPD *vs*. *AE* (Auroral electrojet) index, which is used to describe the activity level of the geomagnetic field. In Figure 11, each little window shows the particle spectrum derived by ASPD in eight azimuths and six pitch angles, these detections show good correlations to the *AE* index. From Figure 11, we found that the plasma particle spectra present good responses to the geomagnetic activities in the polar regions. These results coincide with the natural law of space environment.

3.3.2 Quantitative Test

Due to that it is difficult to find available quantitative da-

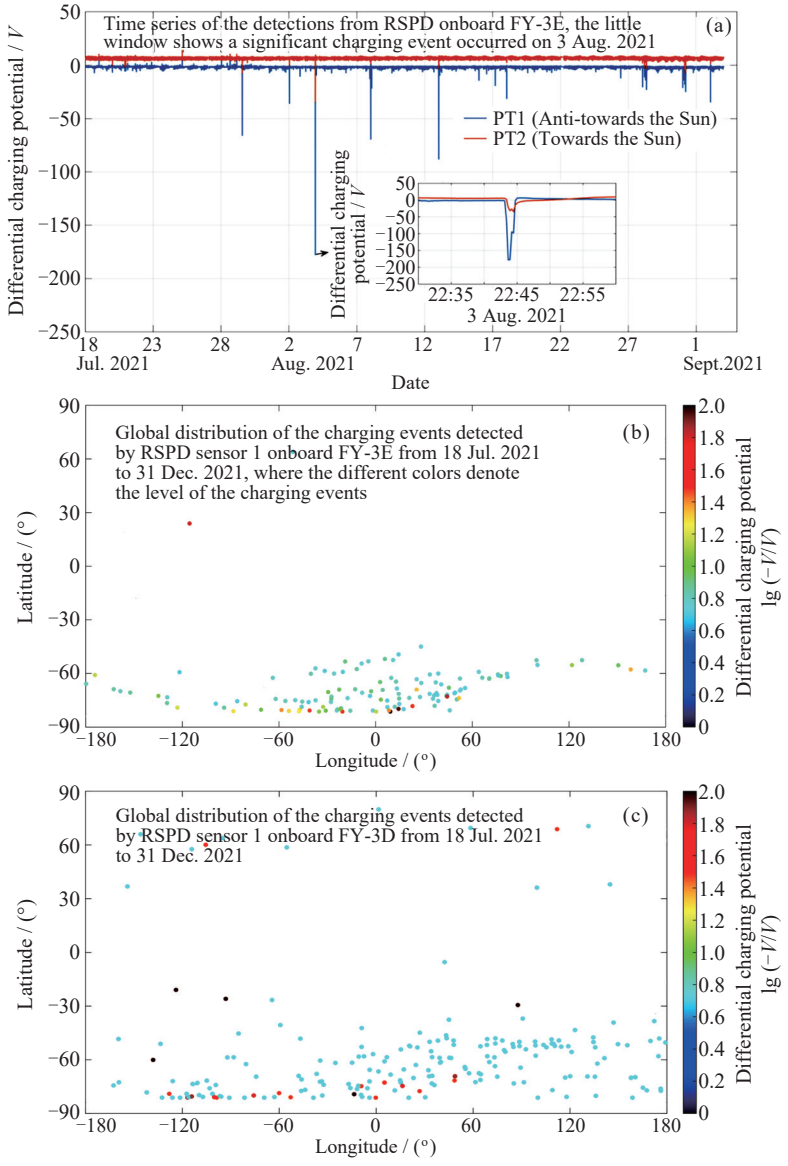
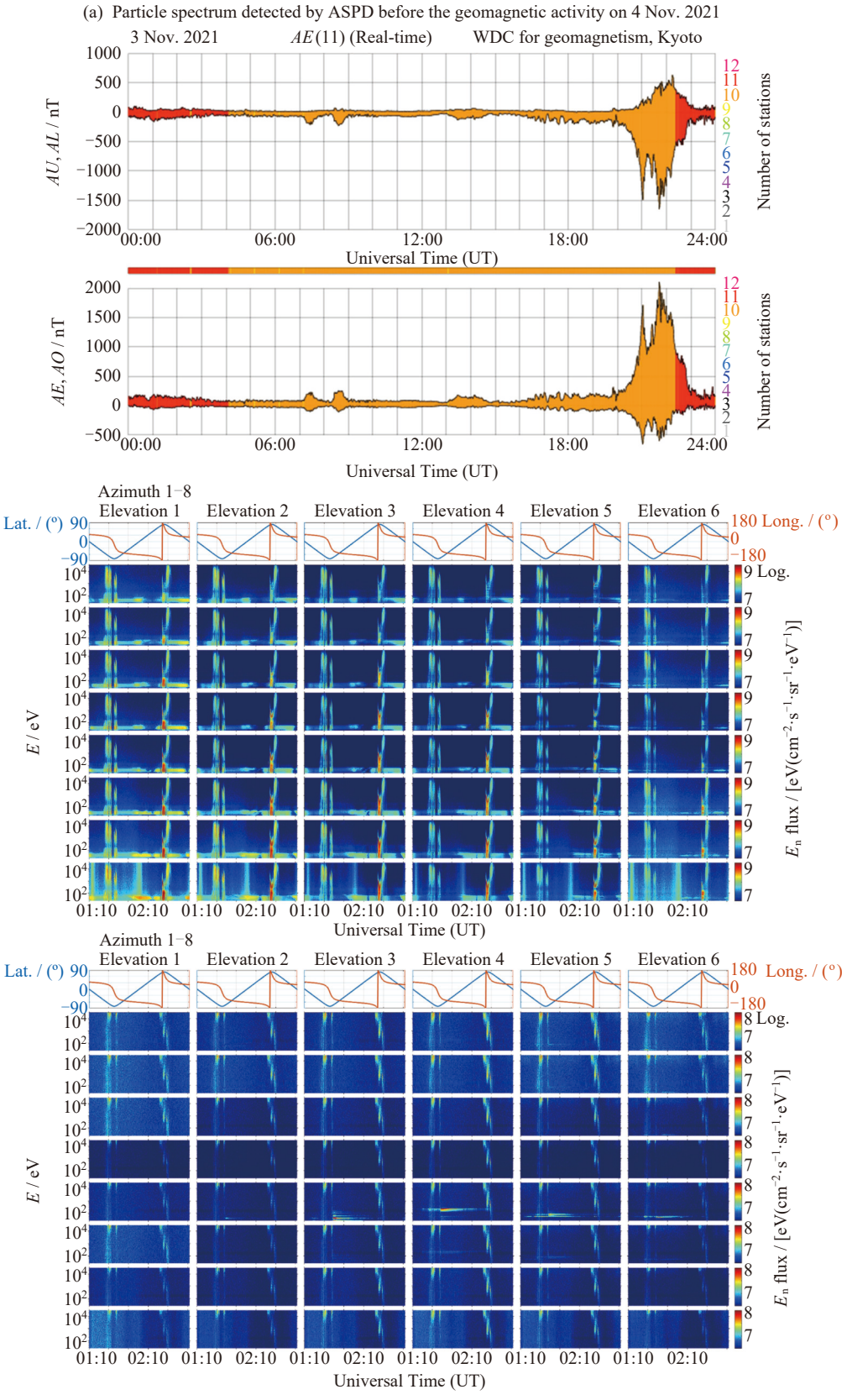


Fig. 10 Charging events observed by RSPD onboard FY-3E and FY-3D


(a) Particle spectrum detected by ASPD before the geomagnetic activity on 4 Nov. 2021
3 Nov. 2021
AE(11) (Real-time)
WDC for geomagnetism, Kyoto
AU, AL / nT
AE, AO / nT
Number of stations
Universal Time (UT)
Azimuth 1–8
Elevation 1
Elevation 2
Elevation 3
Elevation 4
Elevation 5
Elevation 6
Lat. / (°)
Long. / (°)
E / eV
En flux / [eV(cm⁻²·s⁻¹·sr⁻¹·eV⁻¹)]
9 Log.
8 Log.

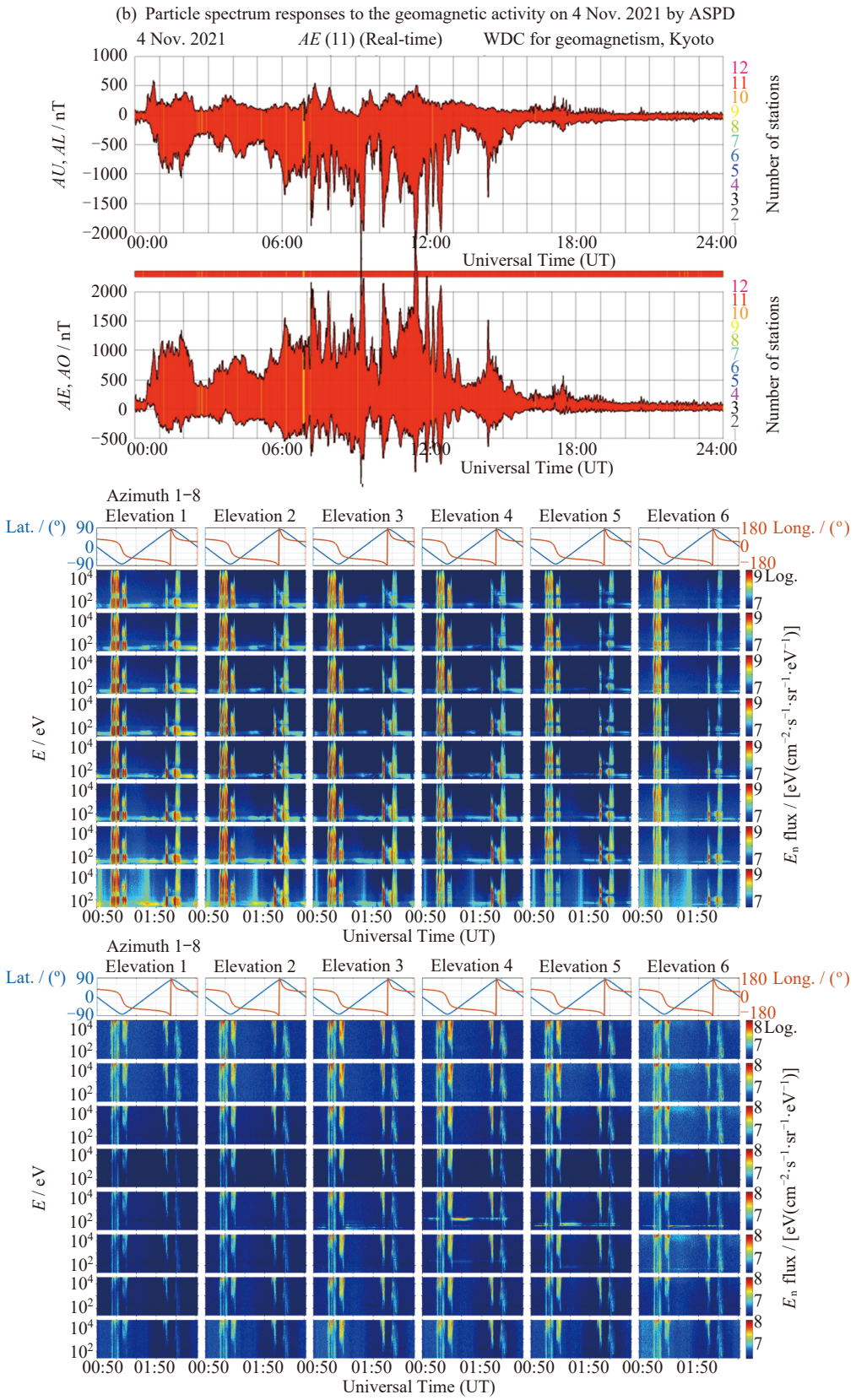
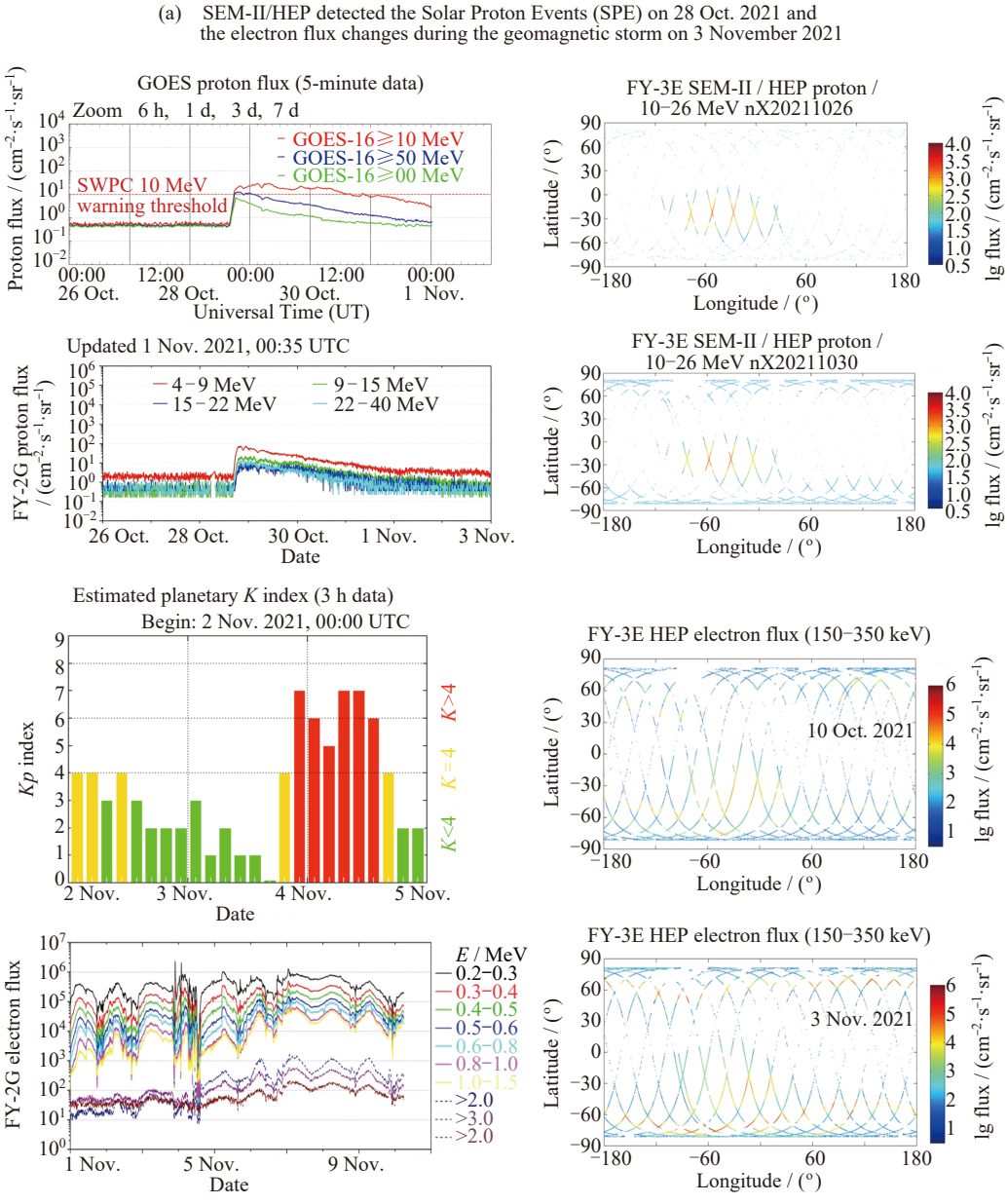


Fig. 11 Plasma spectrum responses to the geomagnetic activity detected by ASPD onboard FY-3E

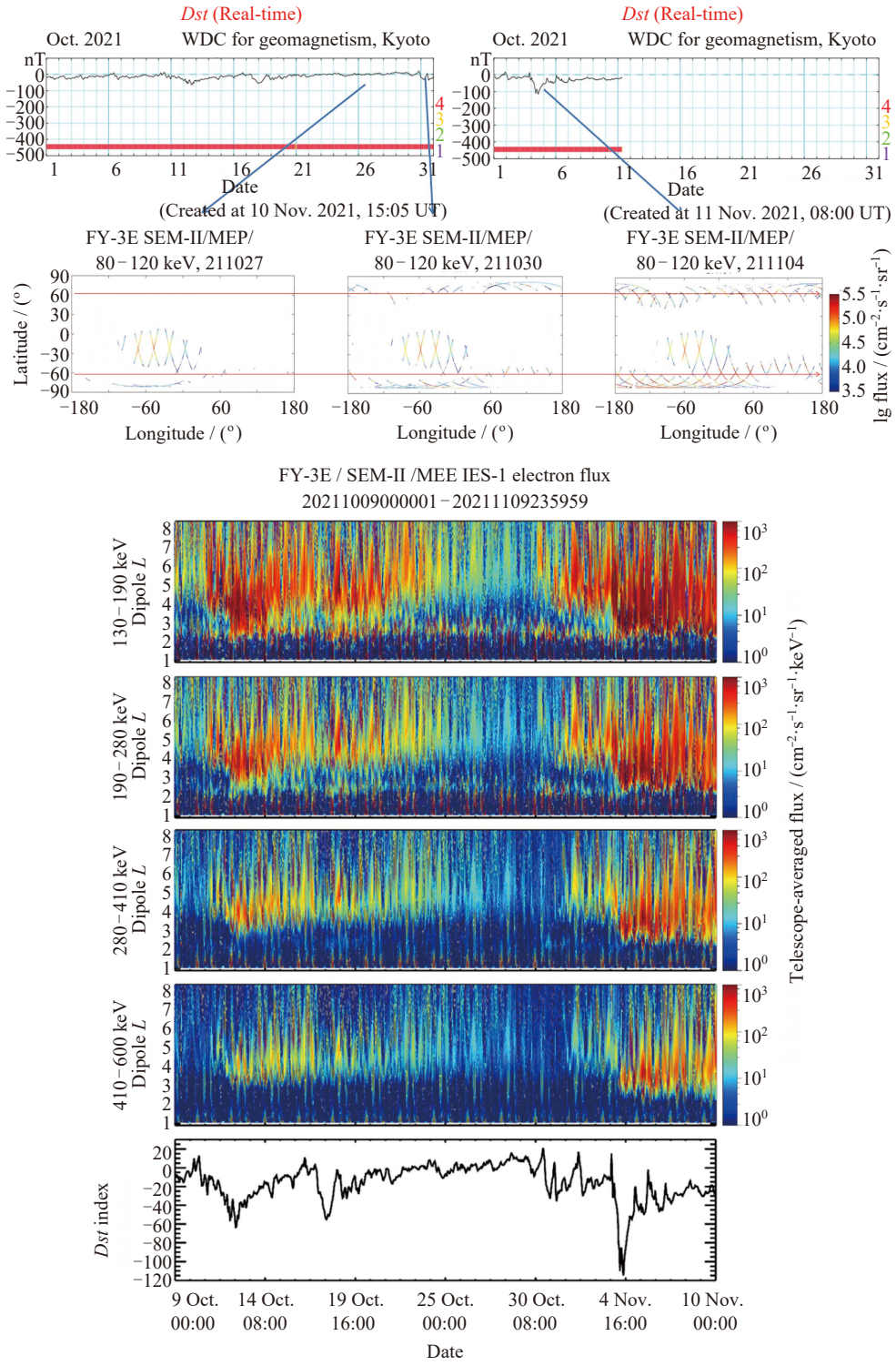
ta source to perform the inter-comparisons of radiation effect detections, we didn't carry out the quantitative test. More detailed discussions for the validation of the radiation dose measurements can be found in Reference [6].

4 Conclusions and Discussions

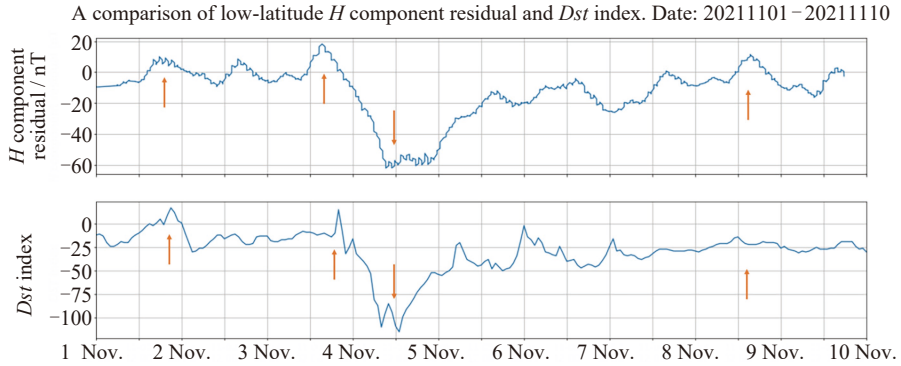
The cross-calibration methods are applied in the in-orbit calibrations and validations of SEM-II. For the particle detectors, we compared the particle detections from SEM-II with the particle detections from MEPED onboard NOAA-POES N-19. For the magnetic field detectors, we compared the magnetic field detections from SEM-II with the outputs from the IGRF13 model. According to the in-orbit calibration results, we derived that the biases of particle detections are within 25% and the magnetic field measurement bias is approximately 1%. We also do the qualitative tests to check if the radiation effect detections follow the natural laws of space environment and the results agree well with our space environment knowledge. The SEM-II detections show good responses to the space weather event that occurred at the end of October, 2021 in Figure 12.



(b) SEM-II/MEP and MEE responses to the *Dst* variations during the space weather activities from late October to early November 2021



(c) SEM-II/MFD responses to the *Dst* changes from 1 to 10 Nov. 2021



(d) SEM-II radiation effect observations during the space weather activities in November 2021

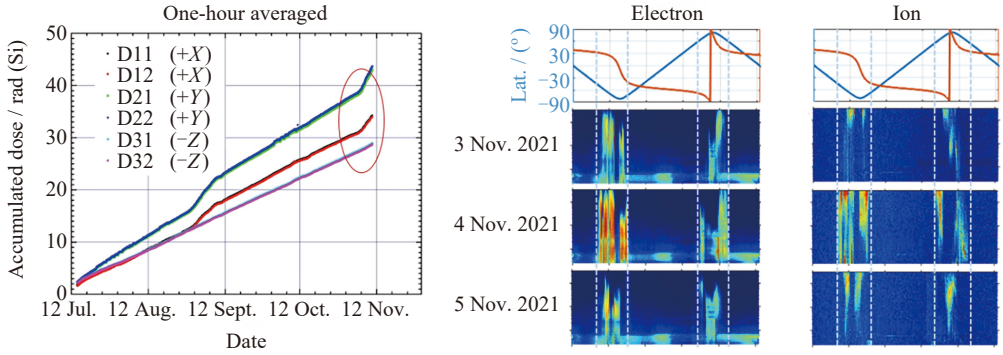


Fig. 12 FengYun-3E/SEM-II responses to the space weather activities occurred from late October to early November 2021

The space environment has significant impacts on satellites or spacecraft, such as energetic charged particles which are a serious concern regarding space weather disasters. When the particles collide on a satellite, energetic electrons can induce surface and deep dielectric charging and cause a possibility of disruption of the satellite's system, and the high-energy protons can penetrate the instruments[7]. Moreover, when these particles precipitate into the ionosphere, energetic electrons and protons produce ionization in the mesosphere and low thermosphere[8], which may produce significant and widespread degradation in short-wave radio propagation, even radio blackouts in extreme cases. In addition, the energetic charged particles also contribute to astronaut radiation exposure, especially in the region of the South Atlantic Anomaly (SAA)[9]. Therefore, it is necessary to monitor the dynamic and anisotropic intensities of the energetic particles is of importance in satellite security designs, investigating the causes of anomalies of satellite systems and degradation of radio communications, and supporting the manned spaceflight missions. The particle detections of space environment also help to develop the radiation belt model, such as AP8/AE8 which were developed to explain the mechanism of the Van Allen radiation belt in the 1970 s[10,11]. However, it is known that AP8 and AE8 models only provide static-average- isotropic particle flux while the geomagnetic field migrates 0.3° every year. Therefore, the outputs of AP8/AE8 models may not be suitable for the requirements in the modern space missions.

Many satellite missions are developed for detecting the radiation belt[12–15]. Currently, the National Oceanic and Atmospheric Administration (NOAA) Polar Orbiting Environmental Satellite (POES) series and China Meteorological Administration's FY-3 series provide the operational measurements of space environment in polar and Sun-synchronous orbits. The information about space environment can be used in space weather forecasting and warning, satellite security designs, satellite malfunction analysis, and scientific studies. We hope

that the data of SEM-II may be applied in more aspects of space science in the future.

Acknowledgements Thanks to the data support from National Satellite Meteorological Center (National Center for Space Weather). Sincere Thanks to Professor XIAO Zuo for his contributions to the space environment exploration in China. We will always cherish the memory of Professor XIAO Zuo.

Ethical Approval This article does not contain any studies with human participants or animals performed by any of the authors.

Conflict of Interests The authors declare that there is no conflict of interests.

References

[1] HUANG C, LI J W, YU T, *et al*. The capabilities and applications of FY-3A/B SEM on monitoring space weather events[J]. *IEEE Transactions on Geoscience and Remote Sensing*, 2012, **50**(12): 4975-4985

[2] WANG C Q, ZHANG X G, LI J W, *et al*. Cross-calibration of high energetic particles data-a case study between FY-3B and NOAA-17[J]. *Science China Technological Sciences*, 2013, **56**(11): 2668-2674

[3] LI J W, HUANG C, YU C, *et al*. Inspection and application of energetic particles data of FY-3C/SEM satellite[J]. *Journal of Remote Sensing*, 2018, **22**(1): 76-86

[4] ZHANG S Y, ZHANG X G, WANG C Q, *et al*. The geometric factor of high energy protons detector on FY-3 satellite[J]. *Science China Earth Sciences*, 2014, **57**(10): 2558-2566

[5] GUBBY R, EVANS J. Space environment effects and satellite design[J]. *Journal of Atmospheric and Solar-Terrestrial Physics*, 2002, **64**(16): 1723-1733

[6] ZHANG B Q, SHEN G H, HUANG C, *et al*. Total ionizing dose measured with the radiation dosimeter onboard the FY-3E satellite[J]. *Journal of Geophysical Research: Space Physics*, 2025, **130**(1): e2024JA033016

[7] Du H, Ye Z H. Space Environment Handbook for LEO Spacecraft[S]. Beijing, China: National Defence Industry Press, 1996 (都亨, 叶宗海. 低轨道航天器空间环境手册 [M]. 北京: 国防工业出版社, 1996)

[8] CODRESCU M V, FULLER-ROWELL T J, ROBLE R G, *et al*. Medium energy particle precipitation influences on the mesosphere and lower thermosphere[J]. *Journal of Geophysical Research: Space Physics*, 1997, **102**(A9): 19977-19987

[9] LI X L, BAKER D N, KANEKAL S G, *et al*. Long term measurements of radiation belts by SAMPEX and their variations[J]. *Geophysical Research Letters*, 2001, **28**(20): 3827-3830

[10] SAWYER D M, VETTE J I. AP-8 Trapped Proton Environment for Solar Maximum and Solar Minimum[R]. Washington: National Aeronautics and Space Administration (NASA), 1976: 76-06

[11] VETTE J I. The AE-8 Trapped Electron Model Environment[R]. Washington: National Aeronautics and Space Administration (NASA), 1991: 91-24

[12] NORTHROP T G, TELLER E. Stability of the adiabatic motion of charged particles in the Earth's field[J]. *Physical Review Journals Archive*, 1960, **117**(1): 215

[13] MCLLWAIN C E. Coordinates for mapping the distribution of magnetically trapped particles[J]. *Journal of Geophysical Research*, 1961, **66**(11): 3681-3691

[14] HESS W. The Radiation Belt and Magnetosphere[M]. Waltham: Blaisdell, 1968

[15] HECKMAN H H, NAKANO G H. Low-altitude trapped protons during solar minimum period, 1962-1966[J]. *Journal of Geophysical Research*, 1969, **74**(14): 3575-3590

Author Biography



HUANG Cong male, born in December 1978 in Jilin City, Jilin Province, is currently the professorate senior engineer and the chief meteorologist at Space Weather Technology Research and Development Division of National Satellite Meteorological Center. His main research direction is space weather monitoring.
E-mail: huangc@cma.gov.cn